Research Article GU J Sci 36(4): 1463-1478 (2023) DOI: 10.35378/gujs.1054803

Gazi University

Journal of Science

http://dergipark.gov.tr/gujs

Alternative Support Material to Platinum Catalyst Used for Oxygen Reduction Reaction: Nonporous Carbon

Aysenur OZTURK[1, *], Ayse BAYRAKCEKEN YURTCAN[2]

[1] *Atatürk University, Chemical Engineering Department, 25240, Erzurum, Turkey*
[2] *Atatürk University, Nanoscience and Nanoengineering Department, 25240, Erzurum, Turkey*

Highlights

- Nonporous carbons were synthesized using different concentrations of HCl.
- The surface areas of the synthesized nonporous carbons were in the range of 19-23 m^2/g.
- All nonporous carbons have negligible micropore volume.
- A maximum limiting current density was -1.2 mA/cm^2 with Pt/nonporous carbon (1 M) catalyst.
- Nonporous carbon shows a low charge transfer resistance in EIS analysis.

Article Info

Received: 07 Jan 2022
Accepted: 28 Sep 2022

Keywords

Nonporous carbon
Acid treatment
Catalyst support
Oxygen reduction reaction

Abstract

In this study, unlike porous carbon as a conventional catalyst support material in fuel cells, nonporous carbon was synthesized in the presence of different HCl concentrations (0.2 M-1 M) and investigated as a support material for platinum (Pt) catalysts in the oxygen reduction reaction (ORR). Since the micropore volume of the synthesized carbons is negligible, the detected surface areas with Brunauer-Emmett-Teller (BET) method were between the range of 19-23 m^2/g. Among the support materials, the carbon-supported Pt catalyst synthesized in the presence of 1 M HCl was investigated electrochemically in terms of hydrogen oxidation (HOR) and ORR half-cell reactions in the three-electrode system. The Pt catalyst supported with nonporous carbon, synthesized using 1 M HCl, reached the maximum limiting current value of -1.2 mA/cm^2 (@1600 rpm, 5 mV/s) at ORR hydrodynamic curves. Low internal and charge transfer resistances of the same catalyst in electrochemical impedance spectroscopy (EIS) analysis are attributable to its nonporous structure.

1. INTRODUCTION

Polymer electrolyte membrane (PEM) fuel cells are hydrogen-based energy converters that attract a lot of attention in transportation, stationary and portable energy systems due to their high energy efficiency and no emission products other than water [1]. In PEM fuel cells, platinum (Pt) is used as a precious metal, which acts as a catalyst for the hydrogen oxidation reaction (HOR) and oxygen reduction reaction (ORR) occurring at the anode and cathode electrodes, respectively. High-cost Pt catalysts are generally employed in conjunction with support materials to reduce their usage amounts. Catalyst supports provide the appropriate electrochemical surface area (ECSA) and electronic conductivity to the catalyst nanoparticles (NPs) [2]. Support materials have a significant effect on fuel cell performance and catalyst durability. So far, easy availability, low cost, high electrical conductivity, and optional structures in many different sizes and properties make carbon derivatives very favorable as catalyst support materials [3]. In our previous fuel cell studies, carbon black (CB) [4], CB-polymer composites [5,6], hollow core mesoporous shell (HCMS) carbon [7,8], carbon nanotubes (CNTs) [9,10], graphene nanoplatelets (GNPs) [11,12], graphene aerogel (GA) [13,14], reduced graphene oxide (rGO) [15], CB-rGO hybrids [16] which are different forms and composites of carbon, were included as catalyst support materials.

Although the utilization of carbon derivatives as catalyst support materials is frequent, they suffer from oxidation in fuel cell operating conditions because the standard potential of the electrochemical oxidation

*Corresponding author, e-mail: abayrakceken@atauni.edu.tr

of carbon is as low as 0.207 V when the normalized hydrogen electrode (NHE) is the reference electrode [17]. If carbon-supported catalysts are used in transportation, challenging conditions such as high water content, low pH (<1), high temperature (50-90 ºC), high working potential (0.6-1.2 V) accelerate carbon corrosion even more. To reach the 5000-hour target of The United States Department of Energy (DOE) for fuel cell durability in 2020, most fuel cell catalysts, support materials, and other components must show high durability. The structural feature of the carbon material highly affects the corrosion rate. Commonly, strategies for reducing carbon corrosion are about modifying the carbon's properties or moderating operating conditions [18].

Porous carbon structures are used for electrochemical applications due to their favorable ECSA values. However, some negative cases can also be encountered in the utilization of porous carbons. The inability to meet the conductive pathways in the porous structure reduces the electrical conductivity. Due to the micropores in the architecture, charge and ion transfer to the electrodes can be delayed, which causes an increase in ohmic resistance. Additionally, some oxygen functional groups such as anhydride, carboxylic, carbonylate, and phenolic are sensitive to pH in porous carbon structures, and this exposes the material to poisoning by organic substances [19]. There are some innovative approaches to the nonporous carbons' synthesis and use in the literature. The catalytic activities of pretreated Vulcan CB-supported Pt NPs were investigated by Kumar et al. [20] for HOR and ORR reactions. Vulcan CB was modified by treating with 5 % HNO_3, 0.07 M H_3PO_4, 0.2 M KOH, and 10 % H_2O_2 and tuning the surface area and micropore volume. 5 % HNO_3 and 10 % H_2O_2 treatment offered significant desulfurization of CB and reduced surface area and micropore volume. Depending on the results, the Pt catalyst with carbon (5 % HNO_3) gave the best HOR activity, while the Pt catalyst with carbon (0.2 M KOH and 10 % H_2O_2) gave the best ORR mass activity. In another study, carbon nanofiber (CNF) and amorphous activated carbon were treated with a strong acid (HNO_3, H_2SO_4) by Guha et al [21]. According to the Brunauer-Emmett-Teller (BET) analysis results, the functionalized CNF had a microporous area corresponding to only 3% of the total surface area, indicating that the structure was nonporous. Yan et al. [22] synthesized nitrogen/phosphorus co-doped nonporous CNF (N/P-NPCNFs) by the electrospinning method of applying polyacrylonitrile (PAN) solutions containing different amounts of H_3PO_4 (5, 10, 20, 30 mass ratios of PAN to H_3PO_4). After stabilization, the produced CNFs were evaluated as supercapacitor electrode material at a high temperature and inert environment. BET surface area of the CNFs differs from each other in the range of 10-65 m^2/g. N/P-NPCNFs-20, which has a 12.2 m^2/g surface area, exhibited the highest specific capacitance (224.9 F/g). Before the carbonization process, Xu et al. [23] transformed internal structure of carbon from microporous to nonporous by applying mechanical pressure to the precursor material. A more ordered graphitic structure, which was substantially free of micropores, was obtained through the mechanical pressure. The authors achieved high Na storage capacity and long-term stability with nonporous carbon while achieving the electrical double layer with microporous carbon for higher capacitance which is substantial for supercapacitors. In this respect, modification of the internal structure of carbon may be beneficial depending on the intended use. In another study, Xu et al. [24] observed that the pore structure of the final carbon formed depending on the degree of polymerization of pyrrole (Py) can be modified in the changing reaction environment. The low and high degree of conjugation of polypyrrole (PPy) with respectively NaOH and HCl resulted in microporous (482 m^2/g) and nonporous (48 m^2/g) structures of carbon frameworks. According to the authors, although the carbon structure synthesized with NaOH is a more suitable electrode material for supercapacitors, the nonporous and less defective carbon structure produced with HCl can also appeal to many applications.

In this study, the idea of observing how the porosity of the structure changes using different acid concentrations has emerged from some studies in the literature. Yakout et al. [25] obtained activated carbon by activating the olive seed with H_3PO_4 at different concentrations (60, 70, 80 wt. %). According to the results of the BET analysis, the mean pore diameter increased with increasing H_3PO_4 concentration. Li et al. [26] treated activated carbon with varying HNO_3 (0.5-67 wt. %) amounts. They found that the 0.5-5 wt. % of HNO_3 improves the structural properties of activated carbon by increasing surface area, total pore volume, and pore diameter but 10-67 wt. % of HNO_3 decreases these parameters. González-García [27] stated that the activation process with high H_3PO_4 concentration triggers the formation of -meso and macropores instead of micropores. On the other hand, carbon activation with alkaline agents supports the

formation of micropores in narrow sizes and large scales. Some studies have already shown that the surface area and micropore volume of carbons activated with KOH increase considerably [28-30].

Porous carbons are preferred as catalyst support material in PEM fuel cells to enhance reactant distribution and water removal. Kong et al. [31] emphasized that the pore size distribution in the gas diffusion layer has a considerable effect on performance than the total porosity. Since catalyst NPs accumulate on the necks of micropores smaller than 2 nm, the pore volume remains inefficient, which does not contribute to the fuel cell performance improvement [32]. Therefore, in this study, it was desired to synthesize nonporous carbon as a fuel cell catalyst support to reduce the micropore volume. The nonporous carbon was synthesized with different concentrations of HCl. Pt NPs supported by nonporous carbon were investigated regarding the ORR activity. Pt NPs can be trapped inside the pores of carbons with large scales micropore volumes. It was aimed to increase Pt utilization efficiency and alleviate the mass transfer problems of species by adopting the nonporous carbon to fuel cell applications. In the literature, the studies include nonporous carbons are dominant for supercapacitors [19,22] instead of fuel cells. This study will be an example of the investigation of ORR activity of nonporous carbon catalyst support for fuel cells. In addition, different concentrations of HCl used in the synthesis of nonporous carbon differentiate the study because the studies are predominantly related to alkaline agents such as KOH. The higher ORR activity can be achieved with less catalyst amount on the support by increasing the efficiency of catalyst utilization in Pt catalysts supported with a nonporous carbon structure. This case reduces the use of Pt, an expensive metal, and allows fuel cells to be less costly. Reducing the costs is a targeted goal, and it is worth the widespread use of hydrogen energy, which is seen as the fuel of vehicles in the future, employing fuel cells.

2. MATERIAL METHOD

2.1. Synthesis of Nonporous Carbon

HCl (Merck, fuming 37 %) solutions with different concentrations were prepared to tailor the porosity of the carbon structure. Five different concentrations of HCl, 0.2 M, 0.4 M, 0.6 M, 0.8 M and 1 M, were used. The procedure implemented by Xu et al. [23] was modified for the nonporous carbon synthesis. 3 ml Py (Sigma Aldrich, ≥ 98 %) was added to 100 ml of HCl solution of different concentrations and stirred for a while. 1820 mg of ammonium persulfate (APS, Sigma Aldrich, 98 %) was added to 100 ml of HCl solution in another beaker. The second solution was poured into the first solution, and the color of the solution changed from light green to black. The final solution was allowed to stir for 2 hours at moderate speed, and was filtered using two pieces of filter paper with a pore size of 125 mm. The solid product was washed with distilled water until the filtrate color changed from green to colorless. After washing, the solid product was left to dry in an oven at 100 ºC for 24 hours under vacuum. Mechanical pressure was applied to the sample for 1 minute after being removed from the furnace. Afterwards, the sample was placed in tube furnace for pyrolysis. Before heating, nitrogen gas was passed through the tube for 10-15 min. Pyrolysis was carried out under continuous nitrogen flow for 3 hours at 800 ºC. After the pyrolysis process, the heating was terminated without stopping nitrogen flow until the furnace temperature dropped to room temperature. The cooled samples were nonporous carbons. Figure 1 schematically shows the synthesis steps of nonporous carbon.

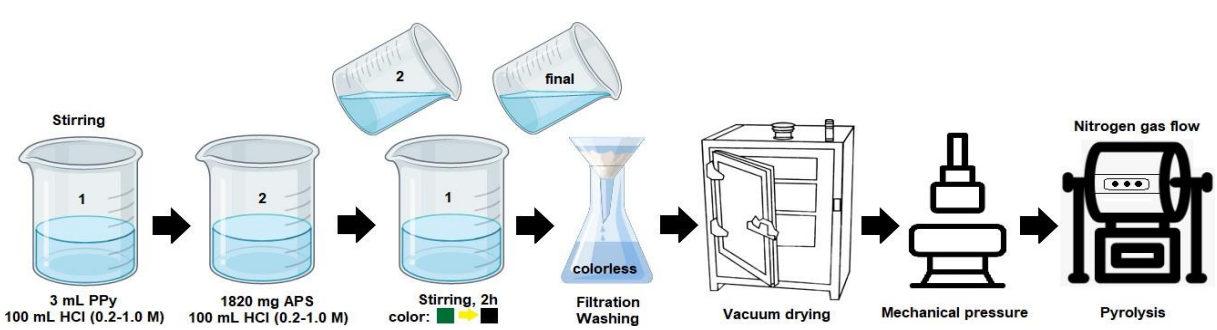

Figure 1. *Synthesis steps of nonporous carbon*

2.2. Microwave Assisted-Polyol Method for Pt Catalyst Preparation

The microwave method is a time-saving and energy-efficient method for obtaining supported catalysts. Generally, ethylene glycol (EG), which has a high capacity to absorb microwave energy and convert it into heat, is preferred as a solvent in this method [33]. In this study, Pt catalyst on nonporous carbon (1 M) by microwave method was loaded as 20 % by mass. In brief, the support material, Pt precursor (hexachloroplatinic acid, H_2PtCl_6, Sigma Aldrich), and EG were combined and mixed. After mixing, the solution was microwaved and left for 1 minute at 800 W. The sample was stacked out from the microwave. It was cooled, centrifuged, washed, and dried [13]. In Figure 2, the Pt NPs reduction procedure on nonporous carbon by microwave-assisted polyol method is given schematically.

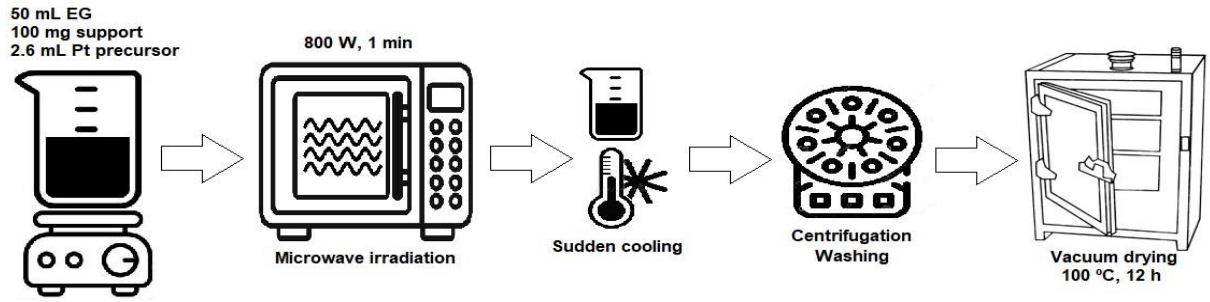

Figure 2. *Microwave-assisted polyol method for the reduction of Pt NPs on nonporous carbon*

2.3. Physical Characterization

Surface areas and pore volumes of nonporous carbons synthesized at different HCl concentrations were determined by BET analysis. The samples were degassed with nitrogen for 8 hours at 250 ºC with a Micromeritics 3Flex device. Raman analysis was conducted for the nonporous carbon (1 M) at 532 nm excitation wavelength by Renishaw inVia device. X-Ray Diffraction (XRD) analysis was performed for nonporous carbon and its Pt catalyst with the PANalytical Empyrean device between 10-90º diffraction angles with a rate of 4º/min. SII Nanotechnology Exstar 7300 (Thermal Gravimetric (TG)-Differential Thermal Gravimetric (DTG)) device was used for thermal characterization of the nonporous carbon (1 M)-supported Pt catalyst. Heating was carried out in the range of 25-1000 ºC in the air atmosphere. Scanning Electron Microscope (SEM) images for nonporous carbon were taken under 15 kV acceleration voltage with Zeiss Sigma 300 model device using different magnifications. Nanoscale images of nonporous carbon loaded with Pt NPs were obtained with the Hitachi HighTech HT7700 model transmission electron microscope (TEM) with lanthanum hexaboride (LaB_6) electron gun. Calculations were made on the TEM image over 50 NPs using ImageJ software to obtain the average size value of the Pt catalyst.

2.4. Electrochemical Characterization

Electrochemical analysis was carried out for nonporous carbon (1 M) and its catalyst in a three-electrode system with a reference electrode (Ag/AgCl), working electrode (glassy carbon (GC, 0.1963 cm^2)), and counter electrode (Pt wire) connected to Ivium potentiostat-galvanostat. The film on the working electrode was obtained by dropping the ink consisting of the relevant support or catalyst, Nafion solution (Ion Power, 15 %), 1,2 propanediol (Sigma Aldrich, ≥99.5 %) and distilled water and drying it at room temperature. Cyclic voltammetry (CV) was performed at different scan rates and cycle numbers in the potential range of -0.28-0.92 V in nitrogen-saturated perchloric acid (0.1 M $HClO_4$) solution. Considering that there is monolayer hydrogen adsorption and desorption between the range of -0.1-0.2 V on the Pt surface, the ECSA was calculated for the Pt catalyst supported by nonporous carbon (1 M) according to the following formula:

$$ECSA = A/K.L.S \; . \qquad (1)$$

A represents the area of the hydrogen desorption peak in the anodic direction, K represents the amount of charge required for hydrogen to cover the Pt surface as a monolayer (0.21 mC/cm^2), L represents the amount of Pt loading on the GC (28 $\mu g/cm^2$) and S, represents the scan rate (20, 50, 100 mV/s) in the Equation (1)

[11]. The ORR activity of the Pt catalyst was investigated by performing a single cycle at a constant scan rate (5 mV/s) between -0.2-0.8 V potentials. The working electrode immersed in the oxygen-saturated 0.1 M $HClO_4$ solution was rotated at certain speeds (100, 400, 900, 1600, 2500 rpm) with the rotator. Finally, electrochemical impedance spectroscopy (EIS) was applied to observe the impedance values formed by the sum of some resistances occurring in electrical circuit components at a constant potential value (0.9 V).

3. RESULTS AND DISCUSSION

3.1. BET

Table 1 lists the structural properties of the nonporous carbons depending on BET analysis. The surface areas of the carbons due to the HCl treatment are substantially low. There was no significant change in the surface areas of nonporous carbons with varying HCl concentrations. Shoaib et al. [34] investigated the change in surface areas for different temperatures and holding times by soaking activated carbon from marine red alga using $ZnCl_2$ in solutions of varying HCl concentrations. Although the HCl concentrations were 1M, 2M, and 3M, the surface areas changed slightly at the same temperature and holding time. The variation range of HCl concentration used in this study is much smaller, so such a result can be acceptable. Additionally, Girgis et al. [35] give the order of activation efficiencies of different inorganic acids for activated carbon obtained from sugarcane bagasse as H_3PO_4>H_2SO_4>HCl>HNO_3, and the surface area of activated carbon obtained by using HCl was the lowest value after HNO_3. Micropore volumes were also small enough (<0.02 cm^3/g) for neglect; this case is evidence of the nonporosity of carbons [19]. Figure 3 shows the nitrogen adsorption/desorption isotherms of the nonporous carbons. Due to the nonporous structure, the volumes adsorbed and desorbed in the samples were low. The isotherms comply with the Type-II isotherm according to the IUPAC classification. This type of isotherm is valid for macroporous or nonporous structures [36]. In this isotherm type, the formation of a monolayer occurs at the beginning of the knee, follows by multi-layer adsorption in the middle of the curve, and ends with capillary condensation occurring at high pressure [37]. Figure 4 is related to the pore size distributions of nonporous carbons. The inside figures show the pore size distribution in a narrower range of pore widths. The pore sizes in carbon samples fall in the 0-20 nm.

Table 1. *BET analysis results of the synthesized nonporous carbons with different acid concentrations*

Support material	**BET surface area (m^2/g)**	**BJH adsorption cumulative volume of pores (cm^3/g)**	**BJH desorption cumulative volume of pores (cm^3/g)**	**BJH adsorption average pore width (nm)**	**BJH desorption average pore width (nm)**
0.2 M	21.2	0.0611	0.0613	11.0	10.9
0.4 M	21.6	0.0620	0.0613	10.9	12.5
0.6 M	22.6	0.0758	0.0746	12.7	14.5
0.8 M	19.8	0.0649	0.0650	12.6	13.1
1 M	23.0	0.0773	0.0763	12.7	14.0

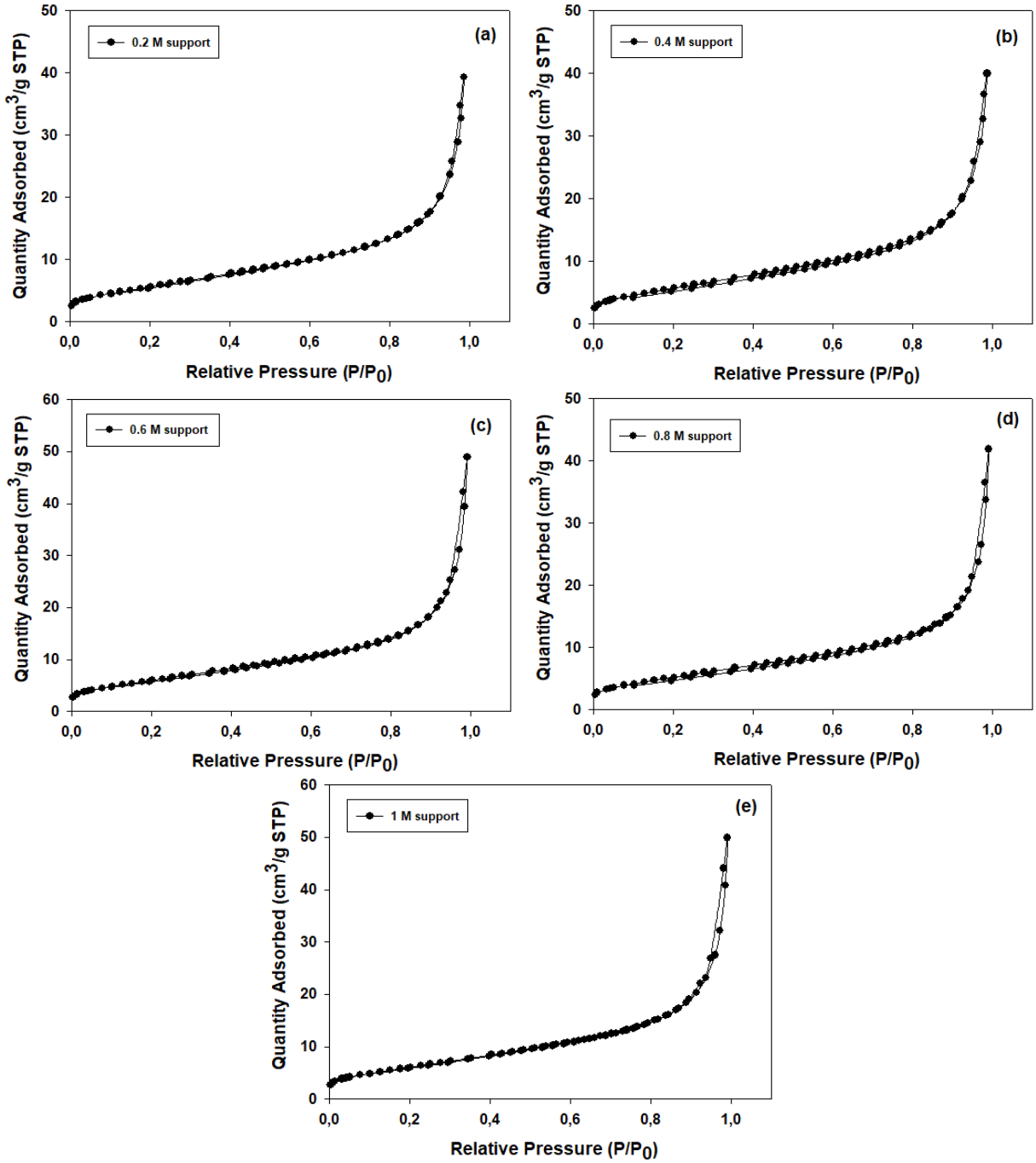

Figure 3. *BET isotherms of the synthesized nonporous carbons with different HCl concentrations*

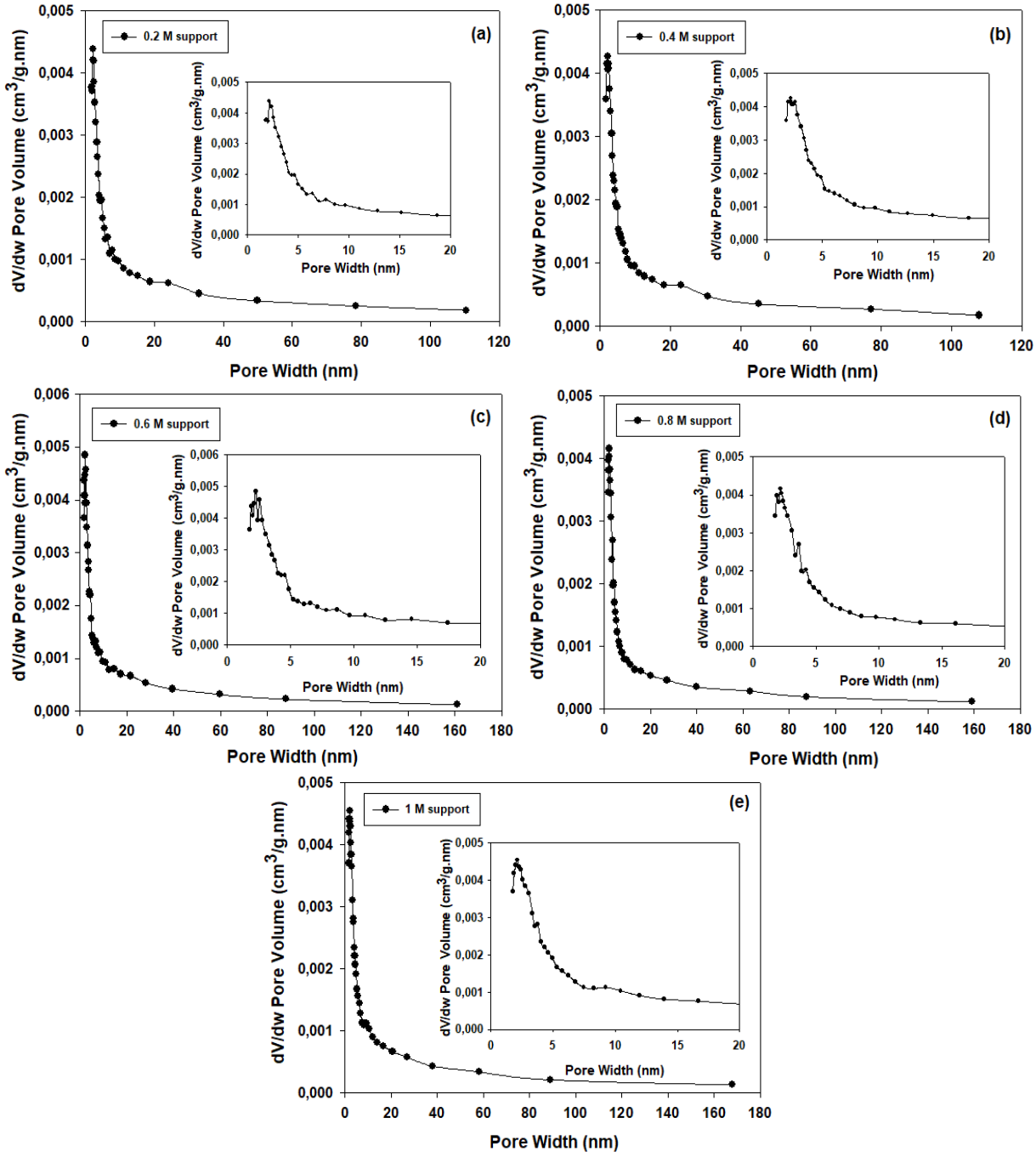

Figure 4. *Pore size distributions of the synthesized nonporous carbons with different HCl concentrations*

3.2. RAMAN & XRD

The Raman analysis of the nonporous carbons is shown in Figure 5(a) The peaks at around 1350 cm^{-1} (D band) and 1580 cm^{-1} (G band) are due to the vibrations of the disordered carbon atoms and sp^2 hybridized carbon atoms in the hexagonal lattice plane, respectively [38]. The ratio of the peak intensities of the two bands (I_D:I_G) were found respectively 0.9877, 0.9717, 0.9695, 0.9677, 0.9613 for the 0.2 M, 0.4 M, 0.6 M, 0.8 M and 1 M HCl treated nonporous carbons. The fact that the D band peak intensity is close to the G band peak intensity indicates the still presence of disorders in the structure. However, as the HCl concentration increases, it is seen that the I_D/I_G ratios slightly decrease. In addition to the D and G bands, the broad peak at around 2700 cm^{-1} represents the 2D band [39]. Since the carbon, synthesized with 1M HCl, has both the highest surface area and the lowest I_D/I_G ratio, the analyses after this section were made only for this sample. The XRD spectra of the nonporous carbon (1 M) and the Pt catalyst were given in Figure 5(b) In the XRD spectrum of the support material, peaks represent the (001), (002) and (100) crystal

planes of graphite [15]. In the XRD spectrum of the Pt catalyst, the characteristic (111), (200), (220), (311) and (222) peaks assign to the face-centered cubic (fcc) crystal planes of the Pt atom [40]. The Debye-Scherrer equation was used to calculate the size of Pt NPs on the support material. The size was determined based on the peak of the Pt (220) plane to avoid the peak broadening due to the overlapping of the carbon (100) and platinum peaks ((111), (200)). The Scherrer equation was given below:

$$D=K.\lambda/\beta.\cos\theta \quad . \tag{2}$$

The components that constitute Equation (2) are respectively: D, Pt crystallite size (nm), K, constant (0.9), λ, the wavelength of X-rays (CuKα: 0.154 nm), β, full width at half maximum (FWHM) value, θ, diffraction angle. The in-plane crystallite size (L_a) (C (100) plane) of the support was calculated from the same equation; however the K constant was 1.84 at this time. The interlayer spacings (C (002) plane) were found from Bragg's Law, which works for finding the lattice spacing of crystals by measuring the wavelength of light [15]. Bragg's law is as follows:

$$n\lambda=2.d.\sin\theta \quad . \tag{3}$$

The symbols in Equation (3) represent n, degree of diffraction maximum (n=1), λ, the wavelength of X-rays (CuKα: 0.154 nm), d, interlayer spacing (nm), and θ, diffraction angle, respectively. Structural parameters of support material and catalyst depending on XRD analysis results were given in Table 2. The interlayer spacings (d_{002}) in both support and catalyst were found as 0.364-0.361 nm, which are higher than the generally accepted value of d_{002} (0.334 nm) in graphite [41]. The in-plane crystalline size (L_a) was 1.95 nm in the support material. The size of Pt NPs loaded on nonporous carbon (1 M) was calculated as 3.99 nm.

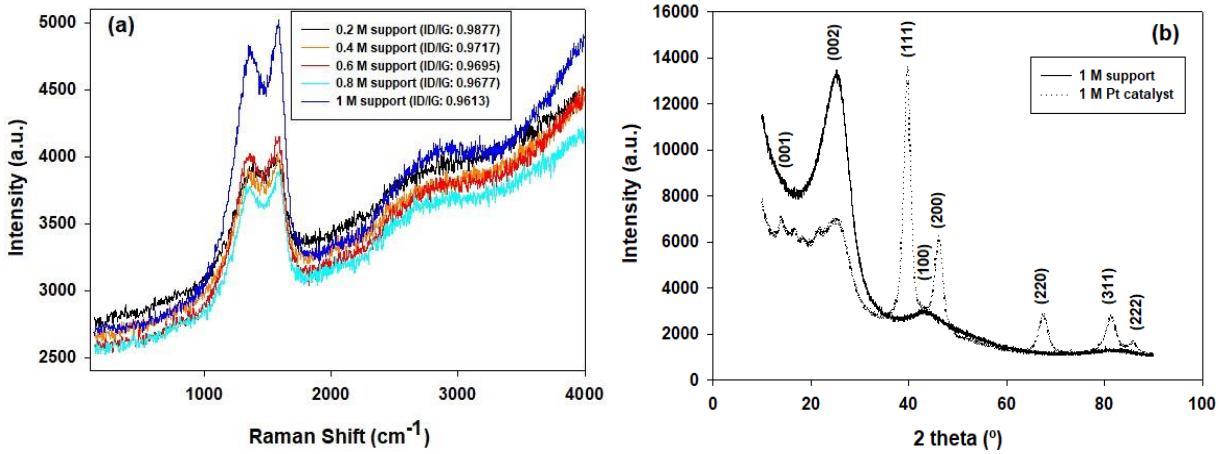

Figure 5. (a) *Raman spectrum of the nonporous carbon supports* ***(b)*** *XRD pattern of the nonporous carbon (1 M) support & nonporous carbon (1 M) supported Pt catalyst*

Table 2. *Structural parameters of nonporous carbon (1 M) support and Pt catalyst*

Sample	d_{002} (nm)	L_a (nm)	Pt particle size (nm)
nonporous carbon (1 M) support	0.364	1.95	-
Pt catalyst	0.361	-	3.99

3.3. TGA & DTG

Figure 6 shows the DTG and TGA curves of the Pt catalyst supported on nonporous carbon (1 M). At the TGA curve of the Pt catalyst, 93.5 % of the total mass remained at 224 ºC. This little mass loss is related to the water removal from the structure. After proceeding to 400 ºC, there was a substantial mass loss due to the thermal decomposition of the material [38]. At 717 ºC, the material reached a plateau in thermal

decomposition pathway, and the remaining mass value was determined as 6.3 %. This mass value is the amount of Pt catalyst that does not undergo thermal degradation on the support material. The earlier thermal degradation of nonporous carbon compared to the widely known Vulcan XC 72R CB may be due to increased defects of the structure as a result of acid treatment [38], [42]. It is seen in the DTG curve that the nonporous carbon gives two peaks at around 400 ºC. This case shows that the mass loss occurred in two consecutive steps [43], and the maximum loss occurred at 462 ºC.

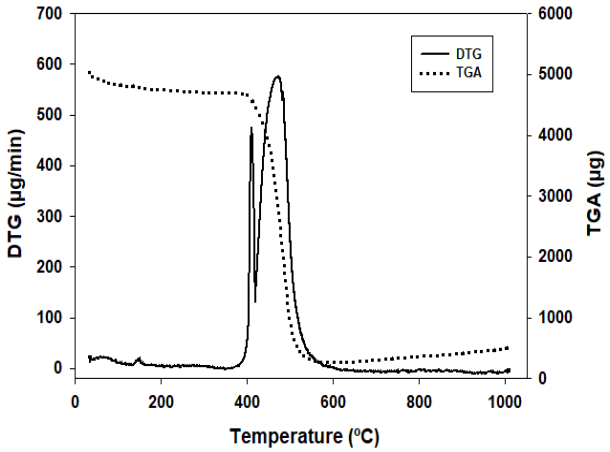

Figure 6. *DTG and TGA analysis of the nonporous carbon (1 M) supported Pt catalyst*

3.4. SEM & TEM

Figure 7 (a-c) demonstrates the SEM images from the nonporous carbon (1 M) surface at different sizes. The dense image of tightly packed carbon spheres reveals the morphological structure [44]. A limited number of voids are present between the carbon clusters. It is evident from the TEM images given in Figure 7. (d-e) that Pt NPs were loaded on nonporous carbon (1 M). Pt NPs were concentrated in some regions. Figure 7. (f) shows the Pt particle size histogram. The mean size of Pt NPs was found to be 3.6 ± 0.65 nm according to the counts made on the TEM image, and this value is close to the previously calculated value (3.99 nm) from the XRD peak.

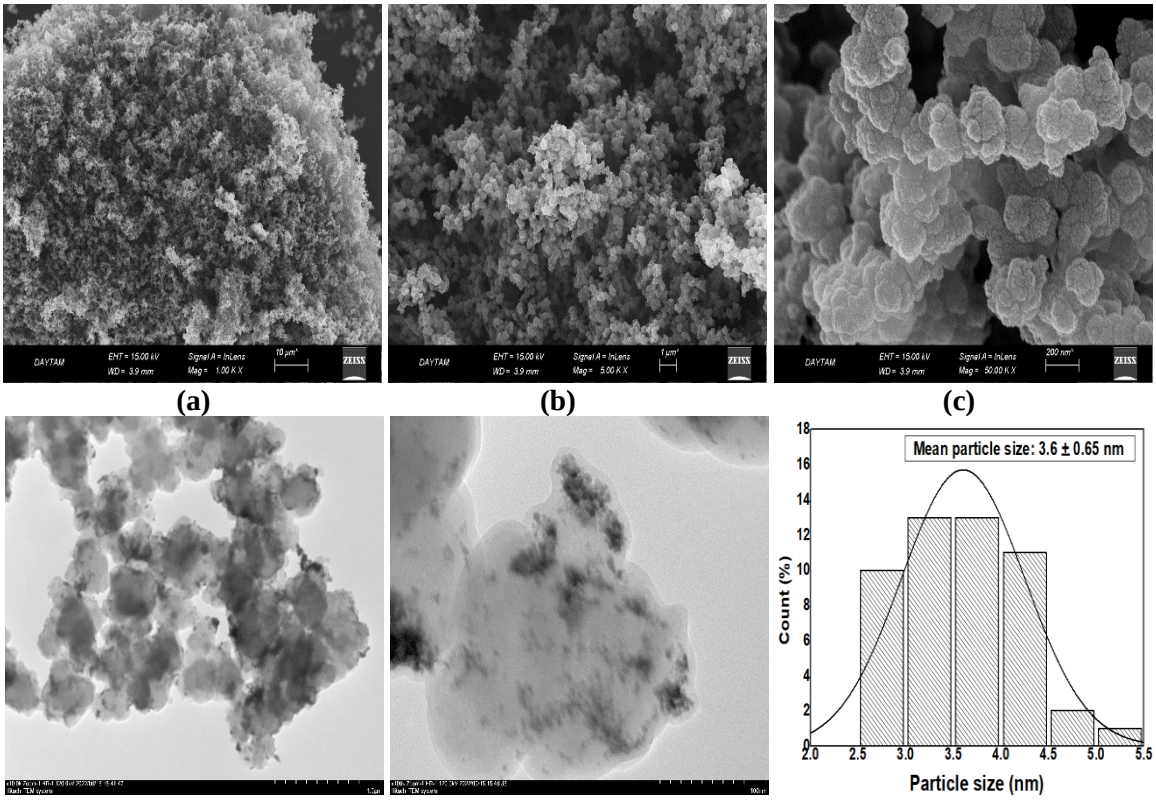

Figure 7. (a-c) *SEM images of the nonporous carbon (1 M)* ***(a)*** *10 µm* ***(b)*** *1 µm* ***(c)*** *200 nm;* ***(d-e)*** *TEM images of the nonporous carbon (1 M) supported Pt catalyst* ***(d)*** *1 µm* ***(e)*** *100 nm;* ***(f)*** *particle size histogram*

3.5. CV & ORR & EIS

Figure 8(a) and Figure 8(b) show the cyclic voltammograms of the support material and the Pt catalyst at different scan rates. In Figure 8. (a), the peak appeared through the oxidation of carbon between 0.3-0.7 V, and the intensity of the peak increased with the increasing scan rate. There are peaks related to the hydrogen adsorption/desorption on the Pt surface in the range of 0.0-0.3 V in the anodic and cathodic directions in Figure 8(b) [45]. The calculated ECSA values based on the hydrogen desorption area were presented in Table 3. The ECSA values at 20, 50, and 100 mV/s were found as 11.9, 21.3, and 25.7 m^2/g, respectively. These values were low due to the nonporous carbon structure. As seen from the narrowing rectangular-shaped CV curves of the Pt catalyst, the nonporous carbon structure exhibited poor capacitive properties [19]. The ORR activity of the Pt catalyst supported by nonporous carbon (1 M) was evaluated by current values measured at different rotational speeds of the rotating disc electrode (RDE) with two different scan rates (5 mV/s & 1 mV/s). The graph of hydrodynamic ORR curves is given in Figure 9 (a-b). It is seen that the limiting current value increases with increasing rotational speed until 1600 rpm. This behavior proves the diffusion inherent to ORR in Pt catalyst [5].

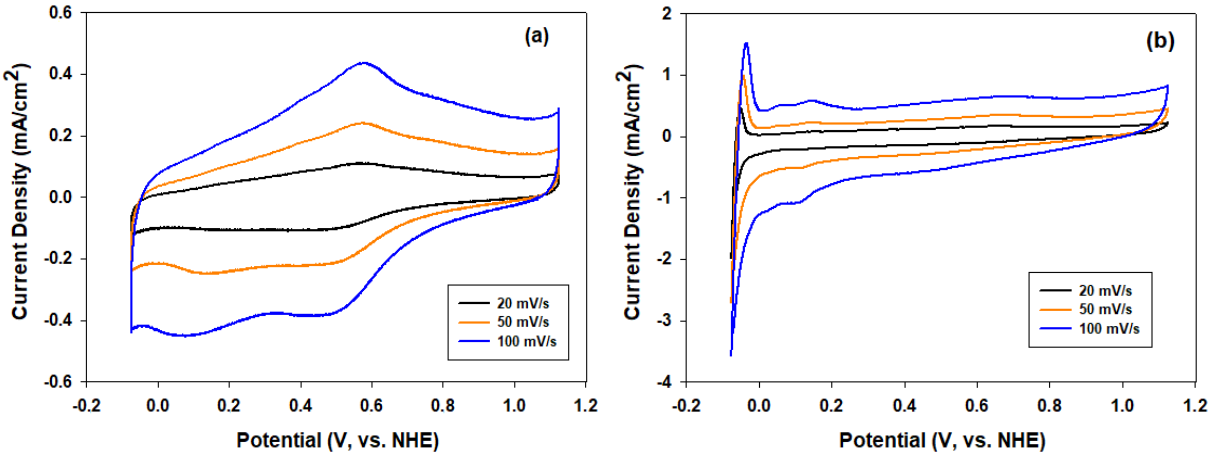

Figure 8. *Cyclic voltammograms* ***(a)*** *nonporous carbon (1 M)* ***(b)*** *nonporous carbon (1 M) supported Pt catalyst*

Table 3. *ECSA values of the nonporous carbon (1 M) supported Pt catalyst at different scan rates*

Scan rate (mV/s)	20	50	100
ECSA (m^2/g)	11.9	21.3	25.7

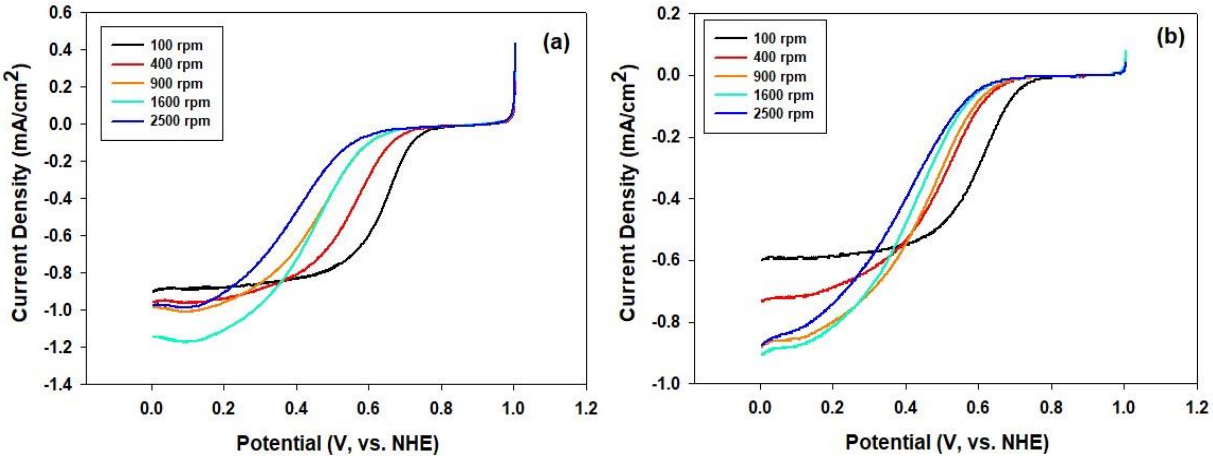

Figure 9. *ORR activity of nonporous carbon (1 M) supported Pt catalyst* ***(a)*** *5 mV/s* ***(b)*** *1 mV/s*

EIS analysis was performed to examine the kinetics at the electrode and electrolyte interface in the frequency range of 1Hz-100 kHz. In Figure 10, the first intersection point on the real axis represents the internal resistance, which is the sum of the electrode, electrolyte, and contact resistances, its value is approximately 6 Ω x cm^2. The small diameter of the semicircle in the high-frequency region of the real axis indicates that the charge transfer resistance is low in both the support material and the Pt catalyst [46]. The numerical values of the charge transfer resistances of the support material and the Pt catalyst are approximately 13 Ω x cm^2 and 17 Ω x cm^2.

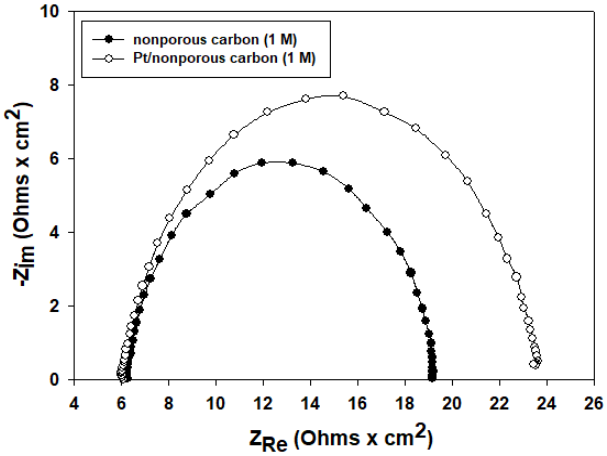

Figure 10. *Nyquist plots of nonporous carbon (1 M) and nonporous carbon (1 M) supported Pt catalyst*

4. RESULTS

In this study, nonporous carbon formed by applying different HCl concentrations, mechanical pressure, and pyrolysis process has been considered support material for fuel cell catalyst. HCl concentrations of 0.2, 0.4, 0.6, 0.8 and 1 M were determined. The synthesized carbons have a BET surface area of 19-23 m^2/g and almost no micropore volume. With Raman analysis, it was understood that there were some structural defects in the nonporous carbon due to the HCl treatment. I_D/I_G ratios of nonporous carbons decreased with increasing HCl concentration. The morphology of the nonporous carbon synthesized with 1 M HCl is a dense structure with fewer voids in the SEM image. Pt precursor was reduced by microwave method on nonporous carbon synthesized with 1 M HCl. The temperature at which the Pt catalyst showed maximum degradation was 462 ºC. In the XRD pattern, peaks belonging to the Pt (fcc) crystal planes of the Pt catalyst appeared. TEM images also proved the loading of Pt catalyst on nonporous carbon. Pt particle sizes calculated from XRD (3.99 nm) and TEM (3.60 nm) analyses agreed with each other. Pt catalyst was tested electrochemically in a three-electrode system. The ECSA value of the Pt catalyst was determined as 21.3 m^2/g at a scanning rate of 50 mV/s. Pt catalyst provided the limiting current value of -1.2 mA/cm^2 at the 5 mV/s scan rate (@1600 rpm). Also, this catalyst has low internal resistance and charge transfer resistance. In this study, a preliminary evaluation was practiced for nonporous carbon. Testing the nonporous carbon in the fuel cell system is envisaged as the next step of this study. By nonporous carbon catalyst support, it is targeted to increase the utilization efficiency of Pt NPs and achieve acceptable fuel cell performances with less catalyst amount.

ACKNOWLEDGEMENTS

The authors acknowledge Atatürk University East Anatolia High Technology Application and Research Center (DAYTAM) for BET, XRD, SEM and TEM analyses, Middle East Technical University Central Laboratory (MERLAB) for Raman analysis and Erzincan Binali Yıldırım University Central Laboratory (EÜTAM) for TGA-DTG analyses.

CONFLICTS OF INTEREST

No conflict of interest was declared by the authors.

REFERENCES

[1] Barbir, F., Yazici, S., "Status and development of PEM fuel cell technology", International Journal of Energy Research, 32: 369-378, (2008).

[2] Jung, N., Chung, D.Y., Ryu, J., Yoo, S.J., Sung, Y.E., "Pt-based nanoarchitecture and catalyst design for fuel cell applications", Nano Today, 9: 433-456, (2014).

[3] Du, L., Shao, Y.Y., Sun, J.M., Yin, G.P., Liu, J., Wang, Y., "Advanced catalyst supports for PEM fuel cell cathodes", Nano Energy, 29: 314-322, (2016).

[4] Bayrakceken, A., Smirnova, A., Kitkamthorn, U., Aindow, M., Turker, L., Eroglu, I., Erkey, C., "Vulcan-Supported Pt Electrocatalysts for PEMFCs Prepared using Supercritical Carbon Dioxide Deposition", Chemical Engineering Communications, 196: 194-203, (2008).

[5] Das, E., Bayrakceken Yurtcan, A., "Effect of carbon ratio in the polypyrrole/carbon composite catalyst support on PEM fuel cell performance", International Journal of Hydrogen Energy, 41: 13171-13179, (2016).

[6] Bozkurt, G., Memioglu, F., Bayrakceken, A., "Pt nanoparticles over PEDOT/carbon composites prepared by supercritical carbon dioxide deposition", Applied Surface Science, 318: 223-226, (2014).

[7] Guvenatam, B., Ficicilar, B., Bayrakceken, A., Eroglu, I., "Hollow core mesoporous shell carbon supported Pt electrocatalysts with high Pt loading for PEMFCs", International Journal of Hydrogen Energy, 37: 1865-1874, (2012).

[8] Ficicilar, B., Bayrakceken, A., Eroglu, I., "Pt incorporated hollow core mesoporous shell carbon nanocomposite catalyst for proton exchange membrane fuel cells", International Journal of Hydrogen Energy, 35: 9924-9933, (2010).

[9] Ozturk, A., Bayrakceken Yurtcan, A., "Synthesis of polypyrrole (PPy) based porous N-doped carbon nanotubes (N-CNTs) as catalyst support for PEM fuel cells", International Journal of Hydrogen Energy, 43: 18559-18571, (2018).

[10] Caglar, A., Cogenli, M.S., Bayrakceken Yurtcan, A., Kivrak, H., "Effective carbon nanotube supported metal (M=Au, Ag, Co, Mn, Ni, V, Zn) core Pd shell bimetallic anode catalysts for formic acid fuel cells", Renewable Energy, 150: 78-90, (2020).

[11] Ozturk, A., Bayrakceken Yurtcan, A., "Raw and pyrolyzed (with and without melamine) graphene nanoplatelets with different surface areas as PEM fuel cell catalyst supports", Carbon Letters, 31: 1191-1214, (2021).

[12] Das, E., Alkan Gursel, S., Isıkel Sanli, L., Bayrakceken Yurtcan, A., "Thermodynamically controlled Pt deposition over graphene nanoplatelets: Effect of Pt loading on PEM fuel cell performance", International Journal of Hydrogen Energy, 42: 19246-19256, (2017).

[13] Oner, E., Ozturk, A., Bayrakceken Yurtcan, A., "Utilization of the graphene aerogel as PEM fuel cell catalyst support: Effect of polypyrrole (PPy) and polydimethylsiloxane (PDMS) addition", International Journal of Hydrogen Energy, 45: 34818-34836, (2020).

[14] Cogenli, M.S., Bayrakceken Yurtcan, A., "Heteroatom doped 3D graphene aerogel supported catalysts for formic acid and methanol oxidation", International Journal of Hydrogen Energy, 45: 650-666, (2020).

[15] Das, E., Ozturk, A., Bayrakceken Yurtcan, A., "Electrocatalytical Application of Platinum Nanoparticles Supported on Reduced Graphene Oxide in PEM Fuel Cell: Effect of Reducing Agents of Dimethlyformamide or Hydrazine Hydrate on the Properties", Electroanalysis, 33: 1721-1735, (2021).

[16] Bayrakceken Yurtcan, A., Das, E., "Chemically synthesized reduced graphene oxide-carbon black based hybrid catalysts for PEM fuel cells", International Journal of Hydrogen Energy, 43: 18691-18701, (2018).

[17] Pethaiah, S.S., Kalaignan, G.P., Ulaganathan, M., Arunkumar, J., "Preparation of durable nanocatalyzed MEA for PEM fuel cell applications", Ionics, 17: 361-366, (2011).

[18] Zhao, J.J., Tu, Z.K., Chan, S.H., "Carbon corrosion mechanism and mitigation strategies in a proton exchange membrane fuel cell (PEMFC): A review", Journal of Power Sources, 488: 229434, (2021).

[19] Hulicova-Jurcakova, D., Kodama, M., Shiraishi, S., Hatori, H., Zhu, Z.H., Lu, G.Q., "Nitrogen-Enriched Nonporous Carbon Electrodes with Extraordinary Supercapacitance", Advanced Functional Materials, 19: 1800-1809, (2009).

[20] Kumar, S.M.S., Hidyatai, N., Herrero, J.S., Irusta, S., Scott, K., "Efficient tuning of the Pt nano-particle mono-dispersion on Vulcan XC-72R by selective pre-treatment and electrochemical evaluation of hydrogen oxidation and oxygen reduction reactions", International Journal of Hydrogen Energy, 36: 5453-5465, (2011).

[21] Guha, A., Lu, W.J., Zawodzinski, T.A., Schiraldi, D.A., "Surface-modified carbons as platinum catalyst support for PEM fuel cells", Carbon, 45: 1506-1517, (2007).

[22] Yan, X.D., Liu, Y., Fan, X.R., Jia, X.L, Yu, Y.H., Yang, X.P., "Nitrogen/phosphorus co-doped nonporous carbon nanofibers for high-performance supercapacitors", Journal of Power Sources, 248: 745-751, (2014).

[23] Xu, F., Qiu, Y.Q., Han, H.J., Jiang, G.S., Zhao, R.X., Zhang, E., Li, H., Wang, H., Kaskel, S., "Manipulation of carbon framework from the microporous to nonporous via a mechanical-assisted treatment for structure-oriented energy storage", Carbon, 159: 140-148, (2020).

[24] Xu, F., Lai, Y.J., Fu, R.W., Wu, D.C., "A facile approach for tailoring carbon frameworks from microporous to nonporous for nanocarbons", Journal of Materials Chemistry A, 1: 5001-5005, (2013).

[25] Yakout, S.M., El-Deen, G.S., "Characterization of activated carbon prepared by phosphoric acid activation of olive stones", Arabian Journal of Chemistry, 9: S1155-S1162, (2016).

[26] Li, J.Y., Ma, L., Li, X.N., Lu, C.S., Liu, H.Z., "Effect of nitric acid, pretreatment on the properties of activated carbon and supported palladium catalysts", Industrial & Engineering Chemistry Research, 44: 5478-5482, (2005).

[27] Gonzalez-Garcia, P., "Activated carbon from lignocellulosics precursors: A review of the synthesis methods, characterization techniques and applications", Renewable & Sustainable Energy Reviews, 82: 1393-414, (2018).

[28] Toprak, A., Kopac, T., "Carbon Dioxide Adsorption Using High Surface Area Activated Carbons from Local Coals Modified by KOH, NaOH and $ZnCl_2$ Agents", International Journal of Chemical Reactor Engineering, 15: 1-16, (2017).

[29] Demiral, H., Demiral, I., "Surface properties of activated carbon prepared from wastes", Surface and Interface Analysis, 40: 612-615, (2008).

[30] Bag, O., Tekin, K., Karagoz, S., "Microporous activated carbons from lignocellulosic biomass by KOH activation", Fullerenes Nanotubes and Carbon Nanostructures, 28: 1030-1037, (2020).

[31] Kong, C.S., Kim, D.Y., Lee, H.K., Shul, Y.G., Lee, T.H., "Influence of pore-size distribution of diffusion layer on mass-transport problems of proton exchange membrane fuel cells", Journal of Power Sources, 108: 185-191, (2002).

[32] Soboleva, T., Zhao, X.S., Mallek, K., Xie, Z., Navessin, T., Holdcroft, S., "On the Micro-, Meso- and Macroporous Structures of Polymer Electrolyte Membrane Fuel Cell Catalyst Layers", ACS Applied Materials & Interfaces, 2: 375-384, (2010).

[33] Bayrakçeken, A., "Platinum or nickel nanoparticles decorated on silica spheres by microwave irradiation technique", Turkish Journal of Chemistry, 38: 309-316, (2014).

[34] Shoaib, A.G.M., El-Sikaily, A., El Nemr, A., Mohamed, A.E.A., Hassan, A.A., "Preparation and characterization of highly surface area activated carbons followed type IV from marine red alga (Pterocladia capillacea) by zinc chloride activation", Biomass Conversion and Biorefinery, 12: 2253-2265, (2022).

[35] Girgis, B.S., Khalil, L.B., Tawfik, T.A.M., "Activated Carbon from Sugar-Cane Bagasse by Carbonization in the Presence of Inorganic Acids", Journal of Chemical Technology and Biotechnology, 61: 87-92, (1994).

[36] Yang, Y.W., Hou, X.Y., Ding, C.F., Lan, J.L., Yu, Y.H., Yang, X.P., "Eco-friendly fabricated nonporous carbon nanofibers with high volumetric capacitance: improving rate performance by tri-dopants of nitrogen, phosphorus, and silicon", Inorganic Chemistry Frontiers, 4: 2024-2032, (2017).

[37] Ambroz, F., Macdonald, T.J., Martis, V., Parkin, I.P., "Evaluation of the BET Theory for the Characterization of Meso and Microporous MOFs", Small Methods, 2: 1800173, (2018).

[38] Dhapola, P.S., Sahoo, N.G., Bhattacharya, B., Kumar, Y., Singh, P.K., Gupta, M., "Elaborative Studies on Non-Porous Carbon Materialfor Super Capacitor Application", Macromolecular Symposia, 388: 1900035, (2019).

[39] Ozturk, A., Ozcelik, N., Bayrakçeken Yurtcan, A., "Platinum/graphene nanoplatelets/silicone rubber composites as polymer electrolyte membrane fuel cell catalysts", Materials Chemistry and Physics, 260: 124110, (2021).

[40] Vengatesan, S., Kim, H.J., Kim, S.K., Oh, I.H., Lee, S.Y., Cho, E., Ha, H.Y., Lim, T-H., "High dispersion platinum catalyst using mesoporous carbon support for fuel cells", Electrochimica Acta, 54: 856-861, (2008).

[41] Niyogi, S., Bekyarova, E., Itkis, M.E., McWilliams, J.L., Hamon, M.A., Haddon, R.C., "Solution properties of graphite and graphene", Journal of the American Chemical Society, 128: 7720-7721, (2006).

[42] Santiago, D., Rodriguez-Calero, G.G., Rivera, H., Tryk, D.A., Scibioh, M.A., Cabrera, C.R., "Platinum Electrodeposition at High Surface Area Carbon Vulcan-XC-72R Material Using a Rotating Disk-Slurry Electrode Technique", Journal of The Electrochemical Society, 157: F189-F195, (2010).

[43] Diaz-Teran, J., Nevskaia, D.M., Lopez-Peinado, A.J., Jerez, A., "Porosity and adsorption properties of an activated charcoal", Colloids and Surfaces A: Physicochemical and Engineering Aspects, 187: 167-175, (2001).

[44] Lin, Q., Peng, X., Zhang, Z., "Electrochemical Determination of Hg(II) Ions Based on Biosynthesized Spherical Activated Carbon from Potato Starch", International Journal of Electrochemical Science, 12: 2232-2241, (2017).

[45] Avcioglu, G.S., Ficicilar, B., Bayrakceken, A., Eroglu, I., "High performance PEM fuel cell catalyst layers with hydrophobic channels", International Journal of Hydrogen Energy, 40: 7720-7731, (2015).

[46] Zhang, M.Y., Yang, C., Wang, Y., Gao, F., Cheng, J., Zhang, J.Y., "High-Performance Supercapacitor Based on Nitrogen and Phosphorus Co-Doped Nonporous Polybenzoxazine-Based Carbon Electrodes", Journal of The Electrochemical Society, 165: A3313-A3320, (2018).